A New Design Framework for Sparse FIR MIMO Equalizers

Ahmad Gomaa, *Student Member, IEEE,* and Naofal Al-Dhahir, *Fellow, IEEE*

***Abstract*—In this paper, we propose a new framework for the design of sparse finite impulse response (FIR) equalizers. We start by formulating greedy and convex-optimization-based solutions for sparse FIR linear equalizer tap vectors given a maximum allowable loss in the decision-point signal-to-noise ratio. Then, we extend our formulation to decision feedback equalizers and multiple-antenna systems. This is followed by further generalization to the channel shortening setup which is important for communication systems operating over broadband channels with long channel impulse responses. We propose a novel approach to design a sparse target impulse response. Finally, as an application of current practical interest, we consider self far-end crosstalk cancellation on vectored very high-speed digital subscriber line systems for cellular backhaul networks.**

***Index Terms*—Sparse FIR filter, MIMO equalizer, DFE, channel shortening, crosstalk.**

I. Introduction

BROADBAND communication channels are characterized by long channel impulse responses (CIRs) that could span tens of symbol periods. Consequently, very long equalizers have to be employed to mitigate the resulting severe inter-symbol interference (ISI). This increases the complexity of computing and implementing (i.e. filtering the received signal) finite impulse response (FIR) equalizers which grows proportional to the number of taps. To reduce complexity at the expense of a tolerable performance loss, long equalizers with few nonzero taps (i.e. sparse equalizers) have been proposed in the literature. In [1], the number of nonzero taps was reduced by choosing only the strongest taps of the minimum mean-squared error (MMSE) linear equalizer (LE). However, the whole equalizer tap vector must be calculated which is computationally complex. The decision feedback equalizer (DFE) was considered in [2] where an ad-hoc algorithm is proposed to determine the locations of the feedforward filter (FFF) taps. In this algorithm, a signal-to-noise ratio (SNR) measure was computed for each channel tap and the FFF taps were assigned to the channel taps with the highest SNRs. Given a fixed total number of DFE taps, the numbers of FFF and feedback filter (FBF) taps were optimized in [3]. Sparse equalization becomes even more critical for multiple-input multiple-output (MIMO) systems [4], [5] where the number of equalizer taps grows proportional to the product of the number of input and output data streams. Greedy and sequential search algorithms were proposed in [6] and [7], respectively, for finding the taps locations for single-input single-output (SISO) LEs and DFEs. In this paper, we present a new framework for designing sparse SISO and MIMO FIR equalizers. Specifically, we formulate both greedy algorithms and l_1-norm minimization programs to determine the locations and weights of the nonzero equalizer taps subject to a given maximum tolerable performance loss. Also, our formulation is not restricted to a specific greedy algorithm as in [6] and [7]. The l_1-norm minimization approach was recently proposed in [8] for sparse FIR filters design subject to a number of constraints on the frequency domain response. However, our sparse equalization problem differs from that in [8] in the formulation, constraints, and applications.

Since equalization complexity increases with the CIR length, a front-end equalizer, commonly known as a channel shortening equalizer (CSE), is designed such that the cascade of the long CIR and the CSE is equivalent to a short target impulse response (TIR). This channel shortening technique enables the implementation of maximum-likelihood (ML) or maximum-a-posteriori (MAP) detectors at practical complexity levels. Several TIR design criteria have been investigated in the literature (see [9] and the references therein). In [9], the unit-tap constraint (UTC) and the unit-energy constraint (UEC) criteria were unified under a single framework that lends itself to other constraints as well. In [10], the CSE designs were generalized to MIMO channels. In [11], the TIR taps were chosen to be noncontiguous and were designed to coincide with the significant multipath arrivals of the original channel. To the best of our knowledge, in all of the previous work, with the exception of [11], the TIR taps were assumed to be contiguous. However, more degrees of freedom and, hence, performance improvement can be obtained by designing the TIR taps to be noncontiguous. In this paper, we allow the TIR taps to be noncontiguous and sparse and formulate both greedy algorithms and l_1-norm minimization programs to determine the locations and values of the sparse taps.

Self far-end crosstalk (FEXT) is a major performance-limiting impairment in vectored very high-speed digital subscriber line (VDSL) systems [12]. The concept of vectored DSL transmission was introduced in [13] where joint signal processing/detection techniques were employed to cancel self FEXT between the vectored DSL lines. Furthermore, it is well-known that most of the self FEXT power emanates from few neighboring lines in the binder. This property was utilized in [14] to reduce the number of nonzero self FEXT cancellation taps whose locations were assigned to the neighboring lines

Paper approved by C. Tepedelenlioglu, the Editor for Synchronization and Equalization of the IEEE Communications Society. Manuscript received April 19, 2010; revised October 12, 2010, February 15, 2011, and March 4, 2011.

This work was supported by RIM Inc. and was presented in part at IEEE GLOBECOM 2010.

The authors are with the University of Texas at Dallas, 2601 N. Floyd Road, Richardson, Texas 75080, USA (e-mail: ahmad.gomaa@utdallas.edu).

Digital Object Identifier 10.1109/TCOMM.2011.09.100231

with the largest average crosstalk power. In this paper, we formulate both greedy algorithms and l_1-norm minimization programs to design a sparse self FEXT canceler subject to a given maximum performance loss from the highly-complex full self FEXT canceler.

The rest of this paper is organized as follows. In Section II, we provide a brief overview of sparse signals recovery techniques. The sparse equalization problem is formulated in Section III. Our sparsity-aware approach for channel shortening is presented in Section IV. In Section V, we describe our approach for partial self FEXT cancellation for vectored VDSL. Finally, simulation results and conclusions are presented in Sections VI and VII, respectively.

Notations: Unless otherwise stated, lower and upper case bold letters denote vectors and matrices, respectively, and $\boldsymbol{A}(:,i)$ denotes the i^{th} column of $\boldsymbol{A}$. The matrices $\mathbf{I}$ and $\mathbf{0}$ denote the identity and all-zero matrices, respectively, and their sizes are denoted by their subscript. Also, $(\ )^H$, $(\ )^*$, $(\ )^{-1}$, and $(\ )^\dagger$ denote the matrix complex-conjugate transpose, complex conjugate, inverse, and pseudo-inverse operations, respectively. The portion of the vector $\boldsymbol{x}$ starting from the index a and ending at the index b is denoted by $\boldsymbol{x}_{a:b}$. The notation $\text{diag}\,(S_1, S_2, \ldots, S_L)$ denotes an $L \times L$ diagonal matrix whose diagonal elements are $\{S_1, S_2, \ldots, S_L\}$. The operators $\| \ . \ \|_0$, $\| \ . \ \|_1$, and $\| \ . \ \|_2$ denote the l_0-norm, l_1-norm, and l_2-norm, respectively. The operators $E\,[.]$ and $|.|$ denote the statistical expectation and the absolute value, respectively.

II. Sparse Signals Recovery Background

Consider the system of equations $\boldsymbol{y} = \boldsymbol{A}\boldsymbol{x} + \boldsymbol{z}$ where $\boldsymbol{y} \in \mathbb{C}^M$ is a known measurement vector, $\boldsymbol{x} \in \mathbb{C}^N$ is an unknown vector, $\boldsymbol{A}$ denotes the $M \times N$ measurement matrix, and $\boldsymbol{z} \in \mathbb{C}^M$ is a bounded noise (error) vector. To obtain the sparsest solution to this system of equations, the following problem is solved

$$\min_{\tilde{\boldsymbol{x}} \in \mathbb{C}^N} \| \tilde{\boldsymbol{x}} \|_0 \quad \text{s.t.} \quad \| \boldsymbol{y} - \boldsymbol{A}\tilde{\boldsymbol{x}} \|_2^2 \leq \epsilon \tag{1}$$

where s.t. means "subject to", ϵ is chosen such that it bounds the amount of noise in the measurements, and $\| \tilde{\boldsymbol{x}} \|_0$ is the number of nonzero entries of $\tilde{\boldsymbol{x}}$. However, in general, finding the optimal solution to this problem is not computationally feasible. Hence, two main approaches have been proposed in the literature to compute a sparse suboptimal solution to this system of equations; specifically, l_1-norm minimization and greedy algorithms. The l_1-norm minimization approach is formulated by replacing $\| \tilde{\boldsymbol{x}} \|_0$ in (1) by $\| \tilde{\boldsymbol{x}} \|_1$. However, the resulting solution is not exactly sparse because many small but nonzero entries will appear in $\tilde{\boldsymbol{x}}$. One method to enforce a finite number of nonzero entries is to apply an additional heuristic optimization step as in [8]. Alternatively, the greedy algorithms provide more control on the set of nonzero elements whose indices and values are determined iteratively. We describe the orthogonal matching pursuit (OMP) algorithm [15] as one of the widely-used greedy algorithms. It takes $\boldsymbol{y}$, $\boldsymbol{A}$, and a certain stopping criterion as its inputs and computes a sparse solution $\tilde{\boldsymbol{x}}$ for the unknown vector $\boldsymbol{x}$ as its output. Hence, we denote the OMP operation by $\tilde{\boldsymbol{x}} = \text{OMP}\ (\boldsymbol{y}, \boldsymbol{A}, \text{stopping criterion})$. The stopping criterion can be a predefined sparsity level (number of nonzero entries) of $\tilde{\boldsymbol{x}}$ or an upperbound on the norm of the residual error term $\| \boldsymbol{y} - \boldsymbol{A}\tilde{\boldsymbol{x}} \|_2$. The OMP algorithm is summarized in the following steps:

Initialization: Define an empty index set $I_0 = \phi$, set the initial residual $\boldsymbol{r}_0 = \boldsymbol{y}$, initialize $\tilde{\boldsymbol{x}} = \mathbf{0}$, and set $k = 1$.

The k^{th} iteration:

1) Compute $\delta_i = \left| \boldsymbol{r}_{k-1}^H \boldsymbol{A}(:,i) \right|$ for all $i \notin I_{k-1}$.
2) Choose $c_k = \arg\max_i \delta_i$.
3) Update $I_k = I_{k-1} \cup c_k$. In this step, the indices of the nonzero elements are augmented by c_k, the index of the k^{th} nonzero entry computed at the k^{th} iteration.
4) Compute $\tilde{\boldsymbol{x}}(I_k) = (\boldsymbol{A}(:, I_k))^\dagger \boldsymbol{y}$ where $\tilde{\boldsymbol{x}}(I_k)$ holds the elements of $\tilde{\boldsymbol{x}}$ indexed by I_k.
5) Compute $\boldsymbol{r}_k = \boldsymbol{y} - \boldsymbol{A}(:, I_k)\tilde{\boldsymbol{x}}(I_k)$ where $\boldsymbol{r}_k$ is the residual error term at the k^{th} iteration.
6) Check the stopping criterion. If met, exit the algorithm, else set $k = k + 1$ and go to Step 1.

In words, OMP tries to find the columns (atoms) of the matrix $\boldsymbol{A}$ (dictionary) whose linear combination is close (matched) to $\boldsymbol{y}$. The orthogonal least squares (OLS) [16] is another greedy algorithm whose initialization step is the same as that of the OMP but the k^{th} iteration is described as follows

1) Implement Steps 3, 4, and 5 in the OMP algorithm for each possible $c_k = i$ such that $i \notin I_{k-1}$ and find c_k and $\tilde{\boldsymbol{x}}(I_k)$ that minimize the resulting residual error term $\| \boldsymbol{r}_k \|_2$.
2) Use $\tilde{\boldsymbol{x}}(I_k)$ from the previous step and implement Step 6 in the OMP algorithm.

Like the OMP algorithm, we denote the OLS algorithm by $\tilde{\boldsymbol{x}} = \text{OLS}\ (\boldsymbol{y}, \boldsymbol{A}, \text{stopping criterion})$. Another greedy algorithm that can be used is the CoSaMP algorithm [17]. Furthermore, it is worth mentioning that the sparse equalization problems considered in this paper are different from the well-known compressed sensing (CS) problem [18]. In CS theory, the measurement matrix $\boldsymbol{A}$ has much fewer rows than columns while, in our problems, as will be shown later, $\boldsymbol{A}$ is either square or tall with full column rank.

III. Sparse FIR Equalization

A. Signal Model

We consider a linear, time-invariant, dispersive, and noisy communication channel with n_i input (transmit) antennas and n_o output (receive) antennas. We use the complex-valued equivalent baseband signal model. Assuming an oversampling factor of l, the received samples at the j^{th} output antenna $(1 \leq j \leq n_o)$ at time k have the form

$$\boldsymbol{y}_k^{(j)} = \sum_{i=1}^{n_i} \sum_{m=0}^{\nu^{(i,j)}} \boldsymbol{h}_m^{(i,j)} x_{k-m}^{(i)} + \boldsymbol{n}_k^{(j)} \tag{2}$$

where $\boldsymbol{y}_k^{(j)}$ is the j^{th} channel output vector, $\boldsymbol{h}_m^{(i,j)}$ is the CIR between the i^{th} input and the j^{th} output whose memory is denoted by $\nu^{(i,j)}$, and $\boldsymbol{n}_k$ is the noise vector at the j^{th} output antenna. All these three quantities are $l \times 1$ vectors corresponding to the l time samples per symbol in the temporally-oversampled channel model. Furthermore, $x_{k-m}^{(i)}$ is the transmitted symbol

from the i^{th} input antenna ($1 \le i \le n_i$). Grouping $\{\boldsymbol{y}_k^{(j)}\}$ into a single $ln_o \times 1$ vector $\boldsymbol{y}_k$ yields

$$\boldsymbol{y}_k = \sum_{m=0}^{\nu} \boldsymbol{H}_m \boldsymbol{x}_{k-m} + \boldsymbol{n}_k \tag{3}$$

where $\boldsymbol{H}_m$ is the $(ln_o \times n_i)$ m^{th} MIMO channel matrix, $\boldsymbol{x}_{k-m}$ is the $n_i \times 1$ input vector at time $k-m$, and $\nu = \max_{i,j} \nu^{(i,j)}$. By grouping $\{\boldsymbol{y}_k\}$ over a block of N_f symbol periods, we express the relation in (3) as follows [4]

$$\boldsymbol{y}_{k:k-N_f+1} = \boldsymbol{H}\boldsymbol{x}_{k:k-N_f-\nu+1} + \boldsymbol{n}_{k:k-N_f+1} \tag{4}$$

where $\boldsymbol{y}_{k:k-N_f+1}$, $\boldsymbol{x}_{k:k-N_f-\nu+1}$, and $\boldsymbol{n}_{k:k-N_f+1}$ are column vectors grouping the received, transmitted, and noise samples over that block. Furthermore, $\boldsymbol{H}$ is a block Toeplitz matrix whose first block row is constructed by the matrices $\{\boldsymbol{H}_m\}_{m=0}^{m=\nu}$ followed by zero matrices. The $n_i\,(N_f+\nu) \times n_i\,(N_f+\nu)$ input correlation matrix is defined by $\boldsymbol{R}_{xx} \triangleq E\left[\boldsymbol{x}_{k:k-N_f-\nu+1}\boldsymbol{x}_{k:k-N_f-\nu+1}^H\right]$, and the $n_o\,(lN_f) \times n_o\,(lN_f)$ noise correlation matrix is defined by $\boldsymbol{R}_{nn} \triangleq E\left[\boldsymbol{n}_{k:k-N_f+1}\boldsymbol{n}_{k:k-N_f+1}^H\right]$. Both $\boldsymbol{R}_{xx}$ and $\boldsymbol{R}_{nn}$ are assumed to be positive-definite correlation matrices. Furthermore, the output-input cross-correlation and the output auto-correlation matrices are given, respectively, by $\boldsymbol{R}_{yx} \triangleq E\left[\boldsymbol{y}_{k:k-N_f+1}\boldsymbol{x}_{k:k-N_f-\nu+1}^H\right] = \boldsymbol{H}\boldsymbol{R}_{xx}$ and $\boldsymbol{R}_{yy} \triangleq E\left[\boldsymbol{y}_{k:k-N_f+1}\boldsymbol{y}_{k:k-N_f+1}^H\right] = \boldsymbol{H}\boldsymbol{R}_{xx}\boldsymbol{H}^H + \boldsymbol{R}_{nn}$.

In the sequel, we show how to design sparse FIR equalizers such that the performance loss does not exceed a predefined limit. In Sections III-B and III-C, we investigate LEs and DFEs, respectively, for SISO systems while in Section III-D, we consider DFEs for MIMO systems with $n_o \ge n_i$.

B. Sparse FIR SISO-LE

In the FIR LE model, the received samples $\{\boldsymbol{y}_k\}$ are applied to a fractionally-spaced FIR equalizer with lN_f taps. The k^{th} error sample is given by

$$e_k = x_{k-\Delta} - \boldsymbol{w}^H \boldsymbol{y}_{k:k-N_f+1} \tag{5}$$

where $\boldsymbol{w}$ is an $lN_f \times 1$ vector of stacked tap weights and Δ is an integer representing the decision delay where $0 \le \Delta \le N_f + \nu - 1$. We use the MMSE criterion to evaluate the equalizer performance. Writing $x_{k-\Delta} = \boldsymbol{I}_\Delta^H \boldsymbol{x}_{k:k-N_f-\nu+1}$ where $\boldsymbol{I}_\Delta$ is the $(\Delta+1)$-th column of $\mathbf{I}_{N_f+\nu}$, the decision-point mean square error (MSE) is given by

$$\xi \triangleq E\left[|e_k|^2\right] = \varepsilon_x - \boldsymbol{w}^H\boldsymbol{r}_\Delta - \boldsymbol{r}_\Delta^H\boldsymbol{w} + \boldsymbol{w}^H\boldsymbol{R}_{yy}\boldsymbol{w} \tag{6}$$

where $\varepsilon_x \triangleq E\left[|x_{k-\Delta}|^2\right]$ and $\boldsymbol{r}_\Delta = \boldsymbol{R}_{yx}\boldsymbol{I}_\Delta$. Defining the Cholesky factorization [19] $\boldsymbol{R}_{yy} \triangleq \boldsymbol{L}\boldsymbol{L}^H$ where $\boldsymbol{L}$ is an $lN_f \times lN_f$ lower-triangular matrix, we rewrite (6) as follows

$$\xi = \varepsilon_x - \boldsymbol{w}^H\boldsymbol{L}\boldsymbol{L}^{-1}\boldsymbol{r}_\Delta - \boldsymbol{r}_\Delta^H\boldsymbol{L}^{-H}\boldsymbol{L}^H\boldsymbol{w} + \boldsymbol{w}^H\boldsymbol{L}\boldsymbol{L}^H\boldsymbol{w} \tag{7}$$

where $(.)^{-H} \triangleq ((.)^H)^{-1}$. Completing the square in (7) yields

$$\xi = \underbrace{\varepsilon_x - \boldsymbol{r}_\Delta^H\boldsymbol{L}^{-H}\boldsymbol{L}^{-1}\boldsymbol{r}_\Delta}_{\triangleq \xi_{\min}} + \underbrace{\|\,\boldsymbol{L}^H\boldsymbol{w} - \boldsymbol{L}^{-1}\boldsymbol{r}_\Delta\,\|_2^2}_{\triangleq \xi_{\text{excess}}} \tag{8}$$

Note that $\boldsymbol{w}$ controls ξ via the term ξ_{excess} only because $\xi_{\min}$ does not depend on $\boldsymbol{w}$. Since $\xi_{\text{excess}} \ge 0$, ξ is minimized by choosing $\boldsymbol{w}$ such that $\xi_{\text{excess}} = 0$ and $\xi = \xi_{\min}$. Consequently, the optimum choice for $\boldsymbol{w}$ in the MMSE sense is

$$\boldsymbol{w}_{\text{opt}} = \boldsymbol{L}^{-H}\boldsymbol{L}^{-1}\boldsymbol{r}_\Delta = \boldsymbol{R}_{yy}^{-1}\boldsymbol{r}_\Delta \tag{9}$$

In general, $\boldsymbol{w}_{\text{opt}}$ is not sparse and, hence, the complexity of computing and implementing $\boldsymbol{w}_{\text{opt}}$ will increase proportional to $(lN_f)^2$ which can be prohibitively large. Any choice for $\boldsymbol{w}$ different from $\boldsymbol{w}_{\text{opt}}$ increases ξ_{excess} which translates into performance degradation. A practical performance-complexity trade-off can be achieved if we design a sparse $\boldsymbol{w}$ such that $\xi_{\text{excess}} \le \epsilon$ where $\epsilon > 0$ controls the tolerable performance loss in terms of MSE increase. According to Section II, this is achieved either by solving the convex optimization program in (10) or by calling the OMP algorithm in (11); i.e.

$$\min_{\boldsymbol{w}_{\text{s}} \in \mathbb{C}^{lN_f}} \|\,\boldsymbol{w}_{\text{s}}\,\|_1 \;\text{ s.t. }\; \|\,\boldsymbol{L}^H\boldsymbol{w}_{\text{s}} - \boldsymbol{L}^{-1}\boldsymbol{r}_\Delta\,\|_2^2 \;\le\; \epsilon \tag{10}$$

$$\boldsymbol{w}_{\text{s}} = \text{OMP}\left(\boldsymbol{L}^{-1}\boldsymbol{r}_\Delta,\, \boldsymbol{L}^H,\, \|\,\boldsymbol{L}^H\boldsymbol{w}_{\text{s}} - \boldsymbol{L}^{-1}\boldsymbol{r}_\Delta\,\|_2^2 \;\le\; \epsilon\right) \tag{11}$$

Since $\boldsymbol{L}$ is a lower-triangular matrix, the vector $\boldsymbol{L}^{-1}\boldsymbol{r}_\Delta$ is easily computed using the forward-substitution method [19]. Note that the matrix $\boldsymbol{L}^H$ is a square matrix, hence this problem is different from the CS setup as pointed out in Section II. In addition, $\boldsymbol{w}_{\text{s}}$ is computed each time the channel estimate is updated. We define the decision-point signal-to-noise ratio as $\widehat{\text{SNR}} \triangleq \frac{\varepsilon_x}{\xi}$ and write $\widehat{\text{SNR}}$ corresponding to $\boldsymbol{w}_{\text{s}}$ as

$$\widehat{\text{SNR}}(\boldsymbol{w}_{\text{s}}) = \frac{\varepsilon_x}{\xi_{\min} + \xi_{\text{excess}}(\boldsymbol{w}_{\text{s}})} \ge \frac{\widehat{\text{SNR}}(\boldsymbol{w}_{\text{opt}})}{1 + \frac{\epsilon}{\xi_{\min}}} \tag{12}$$

where $\widehat{\text{SNR}}(\boldsymbol{w}_{\text{opt}}) \triangleq \frac{\varepsilon_x}{\xi_{\min}}$ and $\xi_{\text{excess}}(\boldsymbol{w}_{\text{s}}) \triangleq \|\,\boldsymbol{L}^H\boldsymbol{w}_{\text{s}} - \boldsymbol{L}^{-1}\boldsymbol{r}_\Delta\,\|_2^2$. The performance loss is quantified by γ where

$$\gamma \triangleq \ell\left(\frac{\widehat{\text{SNR}}(\boldsymbol{w}_{\text{opt}})}{\widehat{\text{SNR}}(\boldsymbol{w}_{\text{s}})}\right) \le \ell\left(1 + \frac{\epsilon}{\xi_{\min}}\right) \triangleq \gamma_{\max} \tag{13}$$

where $\ell(.) \triangleq 10\,\text{Log}_{10}(.)$ and Log_{10} is the base-10 logarithm. To summarize, we compute ϵ based on the acceptable $\gamma_{\max}$ and compute the sparse solution $\boldsymbol{w}_{\text{s}}$ through (10) or (11).

C. Sparse FIR SISO-DFE

For the SISO-DFE, we denote the spans of the FFF, $\boldsymbol{w}$, and the FBF, $\boldsymbol{b}$, by lN_f and N_b taps, respectively. The k^{th} error sample is defined as [20]

$$e_k = x_{k-\Delta} - \left(\boldsymbol{w}^H\boldsymbol{y}_{k:k-N_f+1} - \boldsymbol{b}^H\hat{\boldsymbol{x}}_{k-\Delta-1:k-\Delta-N_b}\right) \tag{14}$$

where $\hat{\boldsymbol{x}}_{k-\Delta-1:k-\Delta-N_b}$ is the slicer output vector representing the hard decisions for $\boldsymbol{x}_{k-\Delta-1:k-\Delta-N_b}$. Assuming correct past decisions, $\hat{\boldsymbol{x}}_{k-\Delta-1:k-\Delta-N_b}$ is replaced by $\boldsymbol{x}_{k-\Delta-1:k-\Delta-N_b}$ and (14) becomes [21]

$$e_k = x_{k-\Delta} - \underbrace{\begin{bmatrix}\boldsymbol{w}^H & -\boldsymbol{b}^H\end{bmatrix}}_{\triangleq \widetilde{\boldsymbol{w}}^H} \underbrace{\begin{bmatrix}\boldsymbol{y}_{k:k-N_f+1} \\ \boldsymbol{x}_{k-\Delta-1:k-\Delta-N_b}\end{bmatrix}}_{\triangleq \tilde{\boldsymbol{y}}} \tag{15}$$

where $\widetilde{\boldsymbol{w}}$ is a length-$(lN_f + N_b)$ vector combining the FFF and the FBF taps. Hence, the MSE ξ is given by

$$\xi = \varepsilon_x - \widetilde{\boldsymbol{w}}^H\tilde{\boldsymbol{r}}_\Delta - \tilde{\boldsymbol{r}}_\Delta^H\widetilde{\boldsymbol{w}} + \widetilde{\boldsymbol{w}}^H\boldsymbol{R}_{\tilde{y}\tilde{y}}\widetilde{\boldsymbol{w}} \tag{16}$$

where $\boldsymbol{R}_{\tilde{y}\tilde{y}} \triangleq E\left[\tilde{\boldsymbol{y}}\tilde{\boldsymbol{y}}^H\right]$, $\tilde{\boldsymbol{r}}_\Delta = \boldsymbol{R}_{\tilde{y}x}\boldsymbol{1}_\Delta$, and $\boldsymbol{R}_{\tilde{y}x} \triangleq E\left[\tilde{\boldsymbol{y}}\,\boldsymbol{x}_{k:k-N_f-\nu+1}^H\right]$. Assuming that $\boldsymbol{R}_{xx} = \varepsilon_x \mathbf{I}_{N_f+\nu}$, it can be shown that [21]

$$\boldsymbol{R}_{\tilde{y}\tilde{y}} = \begin{bmatrix} \boldsymbol{R}_{yy} & \varepsilon_x \boldsymbol{H}\boldsymbol{J}_\Delta \\ \varepsilon_x \boldsymbol{J}_\Delta^H \boldsymbol{H}^H & \varepsilon_x \mathbf{I}_{N_b} \end{bmatrix} \quad \text{and} \quad \boldsymbol{R}_{\tilde{y}x} = \begin{bmatrix} \varepsilon_x \boldsymbol{H} \\ \varepsilon_x \boldsymbol{J}_\Delta^H \end{bmatrix} \tag{17}$$

where $\boldsymbol{J}_\Delta$ is an $(N_f+\nu)\times N_b$ matrix whose structure for $\Delta \le s$ is given by $\boldsymbol{J}_\Delta = \begin{bmatrix}\mathbf{0}_{N_b\times(\Delta+1)} & \mathbf{I}_{N_b} & \mathbf{0}_{N_b\times(s-\Delta)}\end{bmatrix}^H$ with $s \triangleq N_f+\nu-N_b-1$. As in the LE case, we define the Cholesky factorization of $\boldsymbol{R}_{\tilde{y}\tilde{y}}$ as $\boldsymbol{R}_{\tilde{y}\tilde{y}} = \widetilde{\boldsymbol{L}}\widetilde{\boldsymbol{L}}^H$ and write the MSE as follows

$$\xi = \underbrace{\varepsilon_x - \tilde{\boldsymbol{r}}_\Delta^H \widetilde{\boldsymbol{L}}^{-H}\widetilde{\boldsymbol{L}}^{-1}\tilde{\boldsymbol{r}}_\Delta}_{\triangleq \xi_{\min}} + \underbrace{\| \widetilde{\boldsymbol{L}}^H \widetilde{\boldsymbol{w}} - \widetilde{\boldsymbol{L}}^{-1}\tilde{\boldsymbol{r}}_\Delta \|_2^2}_{\triangleq \xi_{\text{excess}}}. \tag{18}$$

where $\widetilde{\boldsymbol{L}}$ depends on Δ. Next, either the convex program in (19) or the OMP algorithm in (20) is used to compute the sparse solution $\widetilde{\boldsymbol{w}}_{\text{s}}$ such that ξ_{excess} does not exceed ϵ; i.e.

$$\min_{\widetilde{\boldsymbol{w}}_{\text{s}}\in\mathbb{C}^{lN_f+N_b}} \| \widetilde{\boldsymbol{w}}_{\text{s}} \|_1 \text{ s.t. } \| \widetilde{\boldsymbol{L}}^H \widetilde{\boldsymbol{w}}_{\text{s}} - \widetilde{\boldsymbol{L}}^{-1}\tilde{\boldsymbol{r}}_\Delta \|_2^2 \le \epsilon \tag{19}$$

$$\widetilde{\boldsymbol{w}}_{\text{s}} = \text{OMP}\left(\widetilde{\boldsymbol{L}}^{-1}\tilde{\boldsymbol{r}}_\Delta,\, \widetilde{\boldsymbol{L}}^H,\, \| \widetilde{\boldsymbol{L}}^H \widetilde{\boldsymbol{w}}_{\text{s}} - \widetilde{\boldsymbol{L}}^{-1}\tilde{\boldsymbol{r}}_\Delta \|_2^2 \le \epsilon\right) \tag{20}$$

After computing $\widetilde{\boldsymbol{w}}_{\text{s}}$, its top lN_f elements are assigned to the FFF and the remaining N_b elements are assigned to the FBF. The quantities γ and $\gamma_{\max}$ can also be defined for the DFE case as in the LE case.

D. Sparse FIR MIMO-DFE

For the FIR MIMO-DFE [4], the length-$(lN_f n_o)$ FFF $\boldsymbol{w}_i$ and the length-$(N_b n_i)$ FBF $\boldsymbol{b}_i$ are designed to recover the i^{th} input stream, i.e. the transmitted stream from the i^{th} input antenna. We assume that only previous decisions on other streams are available at the present time and that these decisions are correct. Then, the k^{th} error sample for the i^{th} input stream $(1 \le i \le n_i)$ is given by [4]

$$e_{k,i} = \boldsymbol{x}_{k-\Delta}(i) - \underbrace{\begin{bmatrix}\boldsymbol{w}_i^H & -\boldsymbol{b}_i^H\end{bmatrix}}_{\triangleq \tilde{\boldsymbol{w}}_i^H} \underbrace{\begin{bmatrix}\boldsymbol{y}_{k:k-N_f+1} \\ \boldsymbol{x}_{k-\Delta-1:k-\Delta-N_b}\end{bmatrix}}_{\triangleq \tilde{\boldsymbol{y}}} \tag{21}$$

where $\boldsymbol{x}_{k-\Delta}(i)$ is the transmitted symbol by the i^{th} input antenna at time $(k-\Delta)$. Note that $\boldsymbol{w}_i$ and $\boldsymbol{b}_i$ are applied, respectively, to the received samples and the decision samples to remove inter-antenna interference. Similar to the SISO-DFE case, the MSE for the i^{th} input stream is

$$\xi_i = \underbrace{\varepsilon_x - \tilde{\boldsymbol{r}}_{\Delta,i}^H \widetilde{\boldsymbol{L}}^{-H}\widetilde{\boldsymbol{L}}^{-1}\tilde{\boldsymbol{r}}_{\Delta,i}}_{\triangleq \xi_{\min,i}} + \underbrace{\| \widetilde{\boldsymbol{L}}^H \widetilde{\boldsymbol{w}}_i - \widetilde{\boldsymbol{L}}^{-1}\tilde{\boldsymbol{r}}_{\Delta,i} \|_2^2}_{\triangleq \xi_{\text{excess},i}} \tag{22}$$

where $\widetilde{\boldsymbol{L}}$ is defined as in the SISO-DFE case and $\tilde{\boldsymbol{r}}_{\Delta,i} = \boldsymbol{R}_{\tilde{y}x}\boldsymbol{1}_{\Delta,i}$ where $\boldsymbol{1}_{\Delta,i}$ is the $(n_i\Delta+i)$-th column of $\mathbf{I}_{n_i(N_f+\nu)}$. To compute a sparse solution $\widetilde{\boldsymbol{w}}_i^H$ such that $\xi_{\text{excess},i} \le \epsilon_i$, we solve the l_1-norm minimization program in (23) or call the OMP algorithm in (24)

$$\min_{\widetilde{\boldsymbol{w}}_{\text{s},i}\in\mathbb{C}^{lN_f n_o+N_b n_i}} \|\widetilde{\boldsymbol{w}}_{\text{s},i}\|_1 \text{ s.t. } \| \widetilde{\boldsymbol{L}}^H \widetilde{\boldsymbol{w}}_{\text{s},i} - \widetilde{\boldsymbol{L}}^{-1}\tilde{\boldsymbol{r}}_{\Delta,i} \|_2^2 \le \epsilon_i \tag{23}$$

$$\widetilde{\boldsymbol{w}}_{\text{s},i} = \text{OMP}\left(\widetilde{\boldsymbol{L}}^{-1}\tilde{\boldsymbol{r}}_{\Delta,i}, \widetilde{\boldsymbol{L}}^H, \|\widetilde{\boldsymbol{L}}^H \widetilde{\boldsymbol{w}}_{\text{s},i} - \widetilde{\boldsymbol{L}}^{-1}\tilde{\boldsymbol{r}}_{\Delta,i}\|_2^2 \le \epsilon_i\right) \tag{24}$$

where $\epsilon_i > 0$ controls the performance loss for the i^{th} input antenna. If the input antennas represent different users with different required quality of service (QoS) levels, the system designer can assign small (large) values of ϵ_i for users demanding high (low) QoS levels, respectively.

IV. Sparse FIR Channel Shortening

For simplicity, we use the signal model in Section III-A with $n_i = n_o = 1$. However, our algorithm can be extended to MIMO systems as well based on the results in [10]. In FIR channel shortening [9], the goal is to design the length-(lN_f) fractionally-spaced CSE, $\boldsymbol{w}$, and the length-$(N_f+\nu)$ TIR, $\boldsymbol{b}$, such that the overall impulse response of the channel and the CSE best approximates a TIR with few, namely (N_b+1), taps. Then, the ML or MAP detectors are designed based on the new short TIR. Although the length of the TIR vector $\boldsymbol{b}$ is $(N_f+\nu)$, only (N_b+1) of its taps are designed to be nonzero. The choice of N_b represents a performance-complexity tradeoff. In [9], the nonzero (N_b+1) taps were chosen to be *contiguous* and their location (delay) within the $(N_f+\nu)$-span of $\boldsymbol{b}$ was optimized. In this paper, we relax the contiguousness constraint and allow the nonzero (N_b+1) taps to be anywhere within the $(N_f+\nu)$-span of the TIR to achieve better performance without increasing complexity. The k^{th} sample of the channel shortening error sequence, e_k, and the channel shortening MSE are given, respectively, by [9]

$$e_k = \boldsymbol{w}^H \boldsymbol{y}_{k:k-N_f+1} - \boldsymbol{b}^H \boldsymbol{x}_{k:k-N_f-\nu+1} \tag{25}$$

$$\begin{aligned}\text{MSE} \triangleq \xi &= E\left[|e_k|^2\right] \\ &= \boldsymbol{w}^H \boldsymbol{R}_{yy}\boldsymbol{w} - \boldsymbol{w}^H \boldsymbol{R}_{yx}\boldsymbol{b} - \boldsymbol{b}^H \boldsymbol{R}_{yx}^H \boldsymbol{w} + \boldsymbol{b}^H \boldsymbol{R}_{xx}\boldsymbol{b}\end{aligned} \tag{26}$$

Minimizing the MSE over $\boldsymbol{w}$ by differentiating it with respect to (w.r.t) $\boldsymbol{w}$ and equating the result to zero, we get $\boldsymbol{w}_{\text{opt}} = \boldsymbol{R}_{yy}^{-1}\boldsymbol{R}_{yx}\boldsymbol{b}$. Substituting $\boldsymbol{w}_{\text{opt}}$ for $\boldsymbol{w}$ in (26), we get

$$\xi = \boldsymbol{b}^H \left(\boldsymbol{R}_{xx} - \boldsymbol{R}_{yx}^H \boldsymbol{R}_{yy}^{-1}\boldsymbol{R}_{yx}\right)\boldsymbol{b} \triangleq \boldsymbol{b}^H \boldsymbol{R}_{x/y}^{\perp}\boldsymbol{b} \tag{27}$$

Minimizing ξ over $\boldsymbol{b}$ yields the trivial solution $\boldsymbol{b} = 0$. To avoid this, we perform the minimization subject to the UTC where one of the (N_b+1) taps is constrained to be unity. The index of the unit tap is denoted by i_t $(0 \le i_t \le N_f+\nu-1)$. Our goal is to design $\boldsymbol{b}$ which minimizes ξ such that its nonzero taps are not constrained to be contiguous unlike [9]. Towards this end, we define the Cholesky factorization [19] of $\boldsymbol{R}_{x/y}^{\perp}$ as $\boldsymbol{R}_{x/y}^{\perp} \triangleq \boldsymbol{U}^H\boldsymbol{U}$ where $\boldsymbol{U}$ is an upper-triangular matrix and rewrite (27) as follows

$$\xi = \boldsymbol{b}^H\boldsymbol{U}^H\boldsymbol{U}\boldsymbol{b} = \| \boldsymbol{U}\boldsymbol{b} \|_2^2 = \| \bar{\boldsymbol{U}}\bar{\boldsymbol{b}} + \boldsymbol{u}_{i_t} \|_2^2 \tag{28}$$

where $\bar{\boldsymbol{U}}$ is formed by all the columns of $\boldsymbol{U}$ except for the i_t^{th} column, $\boldsymbol{u}_{i_t}$, and $\bar{\boldsymbol{b}}$ is formed by all the elements of $\boldsymbol{b}$ except for the i_t^{th} unity element. Observe that the length-$(N_f+\nu-1)$ $\bar{\boldsymbol{b}}$ contains only N_b nonzero taps whose locations and values need to be determined. Hence, we formulate the following convex optimization problem

$$\min_{\bar{\boldsymbol{b}}} \| \bar{\boldsymbol{b}} \|_1 \quad \text{s.t.} \quad \| \bar{\boldsymbol{U}}\bar{\boldsymbol{b}} + \boldsymbol{u}_{i_t} \|_2^2 \le \epsilon_{\text{ch}} \tag{29}$$

where $\epsilon_{\text{ch}} > 0$ is a design parameter that controls the performance. The matrix $\bar{\boldsymbol{U}}$ is a tall matrix, so we have more measurements than unknowns unlike the CS theory setup. Using (29), the designer has no direct control over the resulting number of nonzero taps N_b. Hence, if a specific N_b is desired (e.g. due to complexity constraints), the OLS algorithm[1] is used instead of the above convex program as follows

$$\bar{\boldsymbol{b}} = \text{OLS}\left(-\boldsymbol{u}_{i_t},\ \bar{\boldsymbol{U}},\ \parallel \bar{\boldsymbol{b}} \parallel_0 =\ N_b\right) \tag{30}$$

where $\parallel \bar{\boldsymbol{b}} \parallel_0$ is equal to the number of iterations in the OLS algorithm and the constraint in (30) specifies the number of OLS iterations. After computing $\bar{\boldsymbol{b}}$, we construct the sparse TIR, denoted by $\boldsymbol{b}_{\text{s}}$, by simply inserting the unit tap in the i_t^{th} location. Finally, the optimum (in the MMSE sense) CSE taps and the resulting MMSE are, respectively, found to be

$$\boldsymbol{w}_{\text{opt}} = \boldsymbol{R}_{yy}^{-1}\boldsymbol{R}_{yx}\boldsymbol{b}_{\text{s}}, \quad \xi_{\min} = \boldsymbol{b}_{\text{s}}^H(\boldsymbol{R}_{xx} - \boldsymbol{R}_{yx}^H\boldsymbol{R}_{yy}^{-1}\boldsymbol{R}_{yx})\boldsymbol{b}_{\text{s}} \tag{31}$$

Note that the unit tap index, i_t, needs to be optimized such that the resulting MSE is minimized. However, unlike [9], we do not need to additionally optimize the location of the contiguous taps (i.e. starting index which is commonly known as the decision delay parameter) because we do not constrain the taps to be contiguous. Instead, we use the OLS program in (30) to compute their locations and values. The noncontiguous solution enjoys a larger search space [22] and, hence, the resulting MMSE will be less than (or at least the same as) that of the contiguous solution.

Furthermore, using the same approaches as in Section III, we can design the CSE sparsely [22] to reduce the implementation complexity.

V. Partial Self FEXT Cancellation for Cellular Backhaul in Vectored DSL

A. Signal Model

We consider vectored VDSL [13] transmission with discrete multitone (DMT) modulation for the cellular backhaul application [23]. We assume that L equal-length twisted-pair lines are used to transport traffic from a cellular base station to the backhaul network. The electromagnetic coupling between the vectored twisted-pair lines causes their signals to interfere with each other at the receiver side. This kind of interference is called self far-end crosstalk (FEXT) which is the dominant impairment source in VDSL systems that operate at high frequencies and use short loops. We assume all transmissions are synchronized and employ DMT transmission with a cyclic-prefix whose length equals or exceeds the maximum memory of the direct and crosstalk channels. Grouping the L received signals over the k^{th} tone, we cast the input-output relation as follows [13]

$$\mathbf{Y}^k = \mathbf{H}^k\mathbf{X}^k + \mathbf{Z}^k \tag{32}$$

where $\mathbf{Y}^k$ and $\mathbf{X}^k$ group the L received and transmitted symbols, respectively, on the k^{th} tone. The m^{th} elements of the vectors $\mathbf{Y}^k$ and $\mathbf{X}^k$, denoted by Y_m^k and X_m^k, represent the received and transmitted symbols, respectively, on the m^{th} line at the k^{th} tone. Thermal noise, alien crosstalk, and other impairments experienced by the L lines over the k^{th} tone are lumped and grouped into $\mathbf{Z}^k$. Furthermore, $\mathbf{H}^k$ is the $L \times L$ MIMO channel matrix whose (m,n) element with $m \neq n$, denoted by $H_{(m,n)}^k$, represents the frequency-domain response of the crosstalk channel from the n^{th} line to the m^{th} line at the k^{th} tone. Also, $H_{(m,m)}^k$ represents the direct channel of the m^{th} line at the k^{th} tone.

[1]We found that OLS yields a significantly smaller residual error than OMP especially for small N_f.

B. Partial Self FEXT Cancellation

Self FEXT experienced by the m^{th} line on the k^{th} tone is linearly cancelled by applying $\mathbf{W}_m^k$ such that the estimate of X_m^k is given by $\widetilde{X}_m^k = \left(\mathbf{W}_m^k\right)^H\mathbf{Y}^k$. Dropping the tone index k, for simplicity, and rewriting $\widetilde{X}_m$ in terms of the residual self FEXT interference plus noise, denoted by r_m, we get

$$\begin{aligned}\widetilde{X}_m &= X_m + \left(\mathbf{W}_m^H\mathbf{h}_m - 1\right)X_m + \sum_{n\neq m}\mathbf{W}_m^H\mathbf{h}_nX_n + \mathbf{W}_m^H\mathbf{Z} \\ &\triangleq X_m + r_m\end{aligned} \tag{33}$$

where $\mathbf{h}_n$ is the n^{th} column of $\mathbf{H}$. The residual self FEXT variance is given by

$$\begin{aligned}\zeta_m \triangleq E\left[|r_m|^2\right] &= S_m\left|\mathbf{W}_m^H\mathbf{h}_m - 1\right|^2 + \sum_{n\neq m}S_n\left|\mathbf{W}_m^H\mathbf{h}_n\right|^2 \\ &+ \mathbf{W}_m^H\mathbf{S}_{\mathbf{Z}}\mathbf{W}_m\end{aligned} \tag{34}$$

where $\mathbf{S}_{\mathbf{Z}} \triangleq E\left[\mathbf{Z}\mathbf{Z}^H\right]$ and the lumped noise in $\mathbf{Z}$ is assumed to be uncorrelated with the data. We also assume that $E\left[\mathbf{X}\mathbf{X}^H\right] \triangleq \mathbf{S}_{\mathbf{X}} = \text{diag}\left(S_1, S_2, \ldots, S_L\right)$ where $\{S_m \geq 0, 1 \leq m \leq L\}$ are real numbers. It is easy to show that

$$\begin{aligned}\zeta_m &= \mathbf{W}_m^H\mathbf{S}_{\mathbf{Y}}\mathbf{W}_m - S_m\mathbf{W}_m^H\mathbf{h}_m - S_m\mathbf{h}_m^H\mathbf{W}_m + S_m \\ &= \underbrace{S_m - \bar{\mathbf{h}}_m^H\mathbf{S}_{\mathbf{Y}}^{-1}\bar{\mathbf{h}}_m}_{\triangleq\zeta_{m,\min}} + \underbrace{\parallel \mathbf{L}_{\text{xt}}^H\mathbf{W}_m - \mathbf{L}_{\text{xt}}^{-1}\bar{\mathbf{h}}_m \parallel_2^2}_{\triangleq\zeta_{m,\text{excess}}(\mathbf{W}_m)}\end{aligned} \tag{35}$$

where $\bar{\mathbf{h}}_m = S_m\mathbf{h}_m$ and $\mathbf{S}_{\mathbf{Y}} \triangleq \mathbf{H}\mathbf{S}_{\mathbf{X}}\mathbf{H}^H + \mathbf{S}_{\mathbf{Z}} \triangleq \mathbf{L}_{\text{xt}}\mathbf{L}_{\text{xt}}^H$ where $\mathbf{L}_{\text{xt}}$ is an $L \times L$ lower-triangular matrix. The MMSE canceler is given by $\mathbf{W}_m^{\text{MMSE}} = \mathbf{S}_{\mathbf{Y}}^{-1}\bar{\mathbf{h}}_m$ obtained by setting $\zeta_{m,\text{excess}}(\mathbf{W}_m) = 0$. However, this solution is, generally, nonsparse and requires L multiplications per line per tone per DMT symbol. To reduce run-time complexity, we design a sparse self FEXT cancellation filter $\widehat{\mathbf{W}}_m$ such that $\zeta_{m,\text{excess}}(\mathbf{W}_m) \leq \epsilon_{\text{xt}}$ where $\epsilon_{\text{xt}} > 0$ controls the acceptable data rate loss as will be shown shortly. Again, this is done by either solving the convex program in (36) or calling the OMP algorithm in (37); i.e.

$$\min_{\widehat{\mathbf{W}}_m} \parallel \widehat{\mathbf{W}}_m \parallel_1 \quad \text{s.t.} \quad \parallel \mathbf{L}_{\text{xt}}^H\widehat{\mathbf{W}}_m - \mathbf{L}_{\text{xt}}^{-1}\bar{\mathbf{h}}_m \parallel_2^2 \ \leq \ \epsilon_{\text{xt}} \tag{36}$$

$$\widehat{\mathbf{W}}_m = \text{OMP}\left(\mathbf{L}_{\text{xt}}^{-1}\bar{\mathbf{h}}_m, \mathbf{L}_{\text{xt}}^H, \|\mathbf{L}_{\text{xt}}^H\widehat{\mathbf{W}}_m - \mathbf{L}_{\text{xt}}^{-1}\bar{\mathbf{h}}_m\|_2^2 \leq \epsilon_{\text{xt}}\right) \tag{37}$$

The constraint in (37) can be placed, instead, on the sparsity level (number of active taps) of the canceler if the system is constrained by a certain complexity level. Next, we derive an expression for the data rate loss and show how ϵ_{xt} can be chosen to control this loss. Denoting the tone width by B Hz,

the resulting data rate of the m^{th} line at the k^{th} tone using the designed sparse self FEXT canceler is given from (33) by

$$\begin{aligned} R_m(\widehat{\mathbf{W}}_m) &= B\text{Log}_2\left(1+\frac{S_m/\Gamma}{\zeta_{m,\min}+\zeta_{m,\text{excess}}(\widehat{\mathbf{W}}_m)}\right) \\ &\simeq B\text{Log}_2\left(\frac{S_m/\Gamma}{\zeta_{m,\min}}\right) - B\text{Log}_2\left(1+\frac{\zeta_{m,\text{excess}}(\widehat{\mathbf{W}}_m)}{\zeta_{m,\min}}\right) \\ &\triangleq R_{m,\max} - R_{m,\text{loss}} \end{aligned} \tag{38}$$

where the above approximation is valid since DSL is a high-SNR environment and $R_{m,\text{loss}}$ represents the data rate loss incurred by the sparse self FEXT canceler design. Furthermore, Γ is the SNR gap defined as $\Gamma = \frac{\gamma_m}{3\gamma_c}\left(Q^{-1}(Pe/4)\right)^2$ where γ_c, γ_m, and P_e denote the coding gain, noise margin, and the target bit error-rate, respectively [24]. The function $Q^{-1}(.)$ is the well-known inverse Q-function. Since $\zeta_{m,\text{excess}}(\widehat{\mathbf{W}}_m) \leq \epsilon_{\text{xt}}$ (as ensured by the designs in (36) and (37)), the data rate loss is bounded as $R_{m,\text{loss}} \leq B\text{Log}_2(1+\epsilon_{\text{xt}}/\zeta_{m,\min})$. Hence, ϵ_{xt} is chosen to control the acceptable data rate loss. Furthermore, it has been empirically shown that most of the self FEXT emanates from few neighboring pairs. Hence, the matrix $\bar{\mathbf{H}}$ is sparse and, thus, our proposed technique can effectively cancel most of the self FEXT using substantially fewer taps per tone than those of the MMSE design. We conclude this section by mentioning that we have successfully applied our sparse FIR equalizer design framework to design sparse beamforming antenna arrays to reduce their complexity. Due to lack of space, the details will be reported elsewhere.

VI. Simulation Results

In all the simulations, we use the greedy algorithms[2] described in Section II to obtain the sparse solutions because they, unlike the l_1-norm minimization approach, provide control over the number of nonzero filter coefficients.

A. Sparse Equalization Results

We simulate the performance of our proposed sparse equalizer design for various channel models. For a given $\gamma_{\max}$, we compute the corresponding ϵ via (13), compute the sparse tap weights vector using the OMP algorithm, and calculate the active taps (having nonzero weights) percentage of the total filter span. For example, in SISO-DFEs, the FFF span is lN_f and the FBF span is N_b. When the MMSE solution is used, the number of active filter taps equals the filter span. For LEs, we use $\Delta \approx \frac{N_f+\nu}{2}$ [21], while for DFEs, we use $\Delta = N_f - 1$ which is optimum when $N_b = \nu$ [20]. The noise is modeled as additive white Gaussian with one-sided power spectral density level denoted by N_o. We define the input SNR as $\text{SNR}_\text{I} \triangleq 10\text{Log}_{10}\left(\frac{\varepsilon_x}{N_o}\right)$ and use $N_f = 35$ and $N_b = \nu$.

In Fig. 1, we show the performances of the sparse SISO-DFE and MIMO-DFE for the ITU Vehicular A channel [25] which has a sparse power-delay profile (PDP) with six nonzero paths spanning about eleven symbol durations. For the sparse SISO-DFE, we plot the active FFF taps percentage of lN_f, the active FBF percentage of N_b, and the total active taps percentage of $(lN_f + N_b)$ versus $\gamma_{\max}$ with $l = 2$ samples per symbol. The percentage savings in the FFF tap weights are more than those in the FBF tap weights which is a desirable feature for systems using binary or quadrature phase shift keying (BPSK or QPSK) modulation where the real and imaginary parts of the FBF input are either +1 or -1 thanks to the slicer preceding the FBF. Hence, the FBF operations are simple additions and subtractions, i.e. no multiplications, unlike the FFF whose input samples are continuous-valued. Since $lN_f > N_b$, the total active taps percentage is closer to the active FFF taps percentage than to the FBF taps percentage as shown in Fig. 1. The performance of the sparse MIMO-DFE is also shown in Fig. 1 where the active FFF, FBF, and total taps percentages are plotted versus $\gamma_{\max}$. We observe that allowing a maximum $\widehat{\text{SNR}}$ loss of 0.2dB reduces the total number of active taps by more than 70% for both SISO-DFEs and MIMO-DFEs! Our sparse FIR equalization approach becomes even more advantageous in the MIMO case where the total number of FFF and FBF taps, for the non-sparse solution, increases with $n_i n_o$ and n_i^2, respectively. Comparing the active taps percentages of the SISO-DFE and the MIMO-DFE at the same $\gamma_{\max}$ reveals that the latter needs more taps to mitigate both ISI and inter-antenna interference.

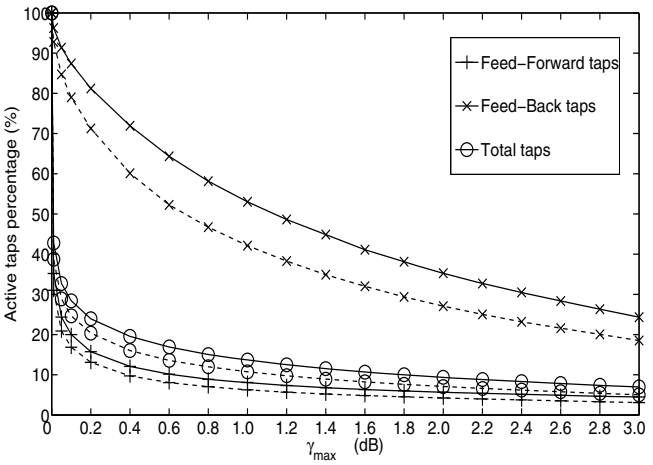

Fig. 1. Active taps percentage versus $\gamma_{\max}$ for SISO-DFEs (dashed lines) and MIMO-DFEs (solid lines) with SNR_I=10 dB for the Vehicular-A channel.

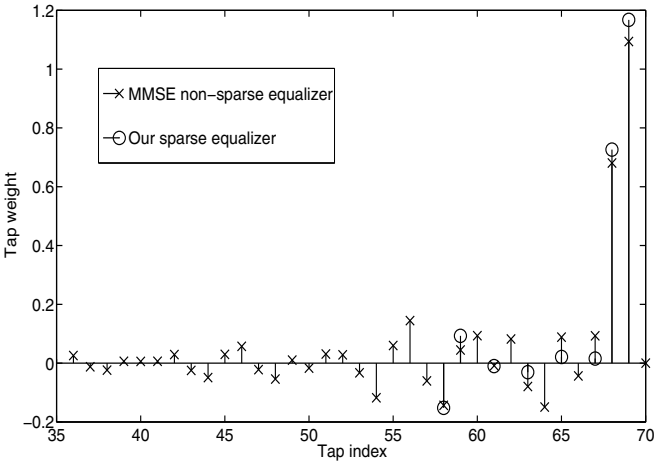

Fig. 2. Single realizations of MMSE and sparse SISO-DFEs FFF impulse responses with SNR_I=25dB and $\gamma_{\max}$=0.3dB for the ITU Vehicular-A channel. The equalizer taps for the indices below 35 are too insignificant to show.

[2]We use OMP for all problems except for finding the TIR taps where we use OLS.

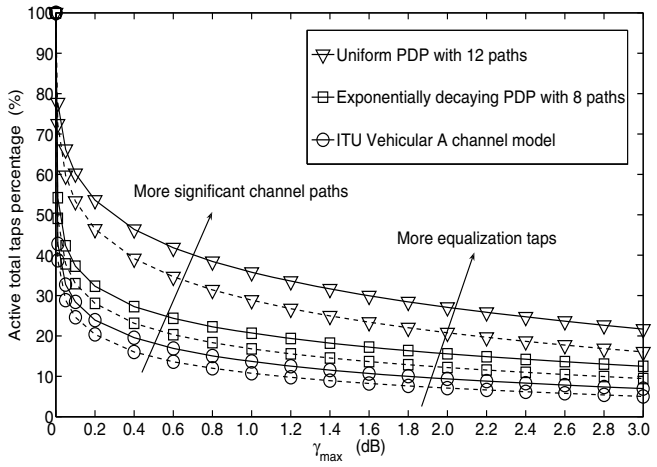

Fig. 3. Active total taps percentage versus $\gamma_{\max}$ for SISO-DFEs (dashed lines) and MIMO-DFEs (solid lines) for various channels with SNR_I=10 dB.

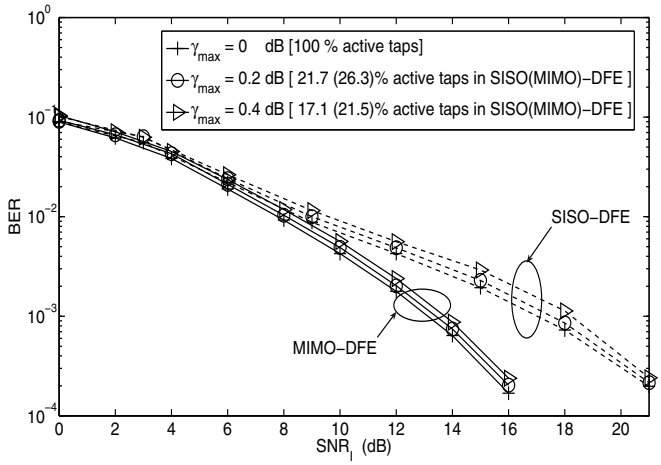

Fig. 4. BER versus SNR_I for SISO-DFEs (dashed lines) with $l = 2$ and for MIMO-DFEs (solid lines) with $n_i = 2$, $n_o = 2$, and $l = 2$. BPSK modulation is used.

Fig. 2 shows a single realization of both the MMSE solution and the sparse solution for SISO-DFEs. The performances of the sparse SISO-DFE and MIMO-DFE are shown in Fig. 3 for non-sparse channel PDPs; namely, a 12-paths uniform PDP and an 8-paths exponentially decaying PDP with a decaying rate of 1 dB per path. On the same figure, we show the performance for the ITU Vehicular A channel for comparison. Inspecting Fig. 3, we observe that as the number of significant paths in the channel PDP increases, more active taps are needed to equalize the channel.

Next, we investigate the bit-error-rate (BER) performance of our sparse FIR equalizers with uncoded BPSK modulation. Both SISO-DFE and MIMO-DFE cases are investigated in Fig. 4 where we plot the BER versus SNR_I for different values of $\gamma_{\max}$. The value $\gamma_{\max} = 0$dB represents the optimum MMSE non-sparse solution where all the equalizer taps are active. For the SISO-DFE case, our sparse design with $\gamma_{\max} = 0.2$ dB and 0.4 dB results in a maximum SNR_I loss of 0.25dB and 0.5dB; however, the number of equalizer taps is reduced by 78.3% and 82.9%, respectively. Furthermore, as expected, the diversity gains of the MIMO-DFE over the SISO-DFE are observed at high values of SNR_I. In Fig. 5, we compare our sparse equalization approach with that in [1] where the whole MMSE

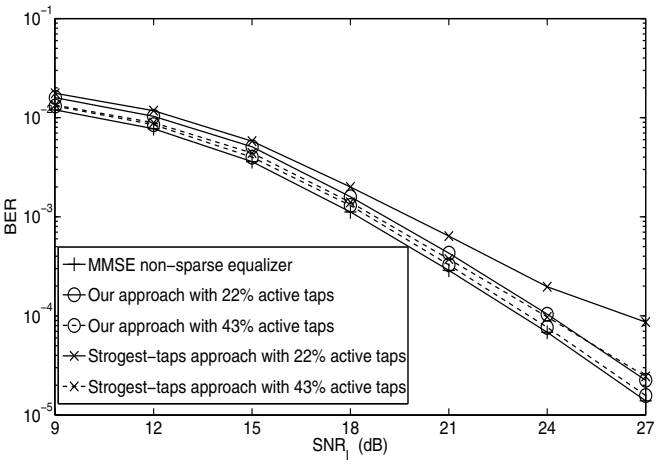

Fig. 5. BER comparison between our sparse equalization approach and the strongest-taps approach for LEs with different sparsity levels (active taps percentages), $l = 2$, and BPSK modulation.

equalizer tap vector is computed but only the F strongest taps are selected. We refer to the approach in [1] as the "strongest-taps" approach. In addition to the performance superiority of our approach compared to the strongest-taps approach, the computational complexity of the latter is less than that of the former where the inversion of an $lN_f \times lN_f$ matrix is required to compute the whole MMSE solution as in (9). However, our OMP-based approach requires the inversion of an $F \times F$ matrix where $F << lN_f$ for all practical purposes.

B. Channel Shortening Results

We simulate the performance of our sparse TIR design and denote the number of nonzero CIR taps by L_{ch}. We compare our sparse TIR design with the TIR design in [11] which we denote by the "strongest-paths" design. Also, we follow the noise model and the input SNR definition in Section VI-A.

The unit tap index, i_t, and the decision delay should be chosen carefully since suboptimum choices can degrade the performance significantly. However, a near optimum performance is achieved with these parameters chosen in the vicinity of $(N_f + \nu)/2$ as shown in [22]. In the rest of simulations, we optimize these parameters to compare the contiguous, strongest-paths, and our sparse noncontiguous TIR designs. In Fig. 6, we plot $\text{SNR}_\text{o}(\boldsymbol{w}_{\text{opt}})$ versus N_f for the ITU Vehicular A channel with N_b ranging from 1 (lower curves) to $L_{\text{ch}} - 1$ (upper curves). Recall that $(N_b + 1)$ represents the number of TIR taps. As N_b increases, the output SNR increases for all TIR designs as expected which means that the TIR becomes more accurate in approximating the actual CIR. However, we observe that our sparse noncontiguous design of the TIR performs better than the other designs for all choices of N_f and N_b. Results for nonsparse channels are shown in [22]. From Fig. 6, we observe that our sparse design with $N_b = 3$ outperforms both the contiguous MMSE and the strongest-paths designs with $N_b = 5$ over the whole range of N_f and for $N_f \geq 30$, respectively. Therefore, allowing the TIR taps to be noncontiguous results in a better performance at the same complexity (measured by N_b) or in a lower complexity at the same performance. The complexity is measured by N_b because the number of TIR trellis states (directly impacts the

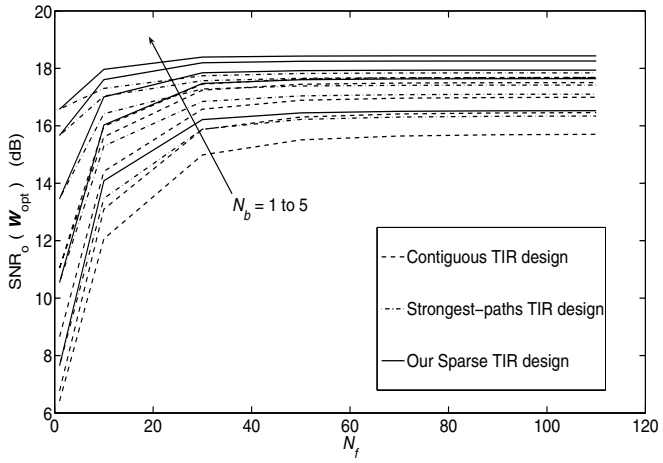

Fig. 6. $\mathrm{SNR_o}(\boldsymbol{w}_{\mathrm{opt}})$ versus N_f for three TIR designs for Vehicular A CIR with $\mathrm{SNR_I} = 20$ dB.

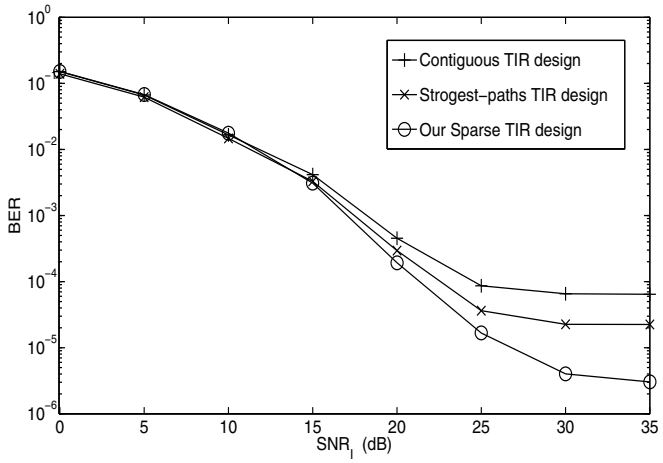

Fig. 7. BER versus $\mathrm{SNR_I}$ for various TIR designs with MLSE detection for Vehicular A CIR with $N_f = 40$, $N_b = 3$, and BPSK modulation.

ML/MAP detectors complexity) increases exponentially with N_b. The number of states for the contiguous design is $2^{(N_b+1)}$. Although the number of trellis states for the noncontiguous TIR design is larger than that for the contiguous one due to the spread of the TIR taps, the algorithm in [26] can be employed to reduce the number of computations. Alternatively, the belief propagation (BP) algorithm can be used since its complexity is exponential only in N_b regardless of the nonzero taps locations [11]. However, the BP algorithm suffers from short cycles which impact the accuracy of the messages independence assumption. In our simulations, we use the ML (BP) algorithm if the span of nonzero TIR taps is less (greater) than the maximum capacity of the simulation tool, respectively.[3] The superiority of our sparse TIR design over the contiguous and strongest-taps TIR designs is evident in Fig. 7 where the former outperforms the contiguous and strongest-taps designs by about 3.3 dB and 1.3 dB, respectively, at BER $\approx 10^{-4}$. Furthermore, both contiguous and strongest-taps designs reach their error floors earlier than our sparse TIR design where the error floors in Fig. 7 are due to the residual channel shortening MSEs. Furthermore, our sparse TIR design reduces the error floor by about one order of magnitude compared to the strongest-paths TIR designs and by more than one order of magnitude compared to the contiguous TIR design.

[3]BP is not used by itself to reduce the impact of short cycles.

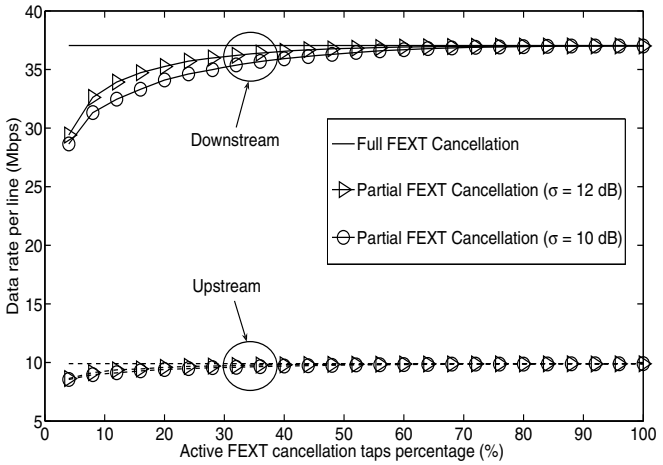

Fig. 8. Achievable downstream (solid lines) and upstream (dashed lines) data rates per line versus active taps percentage for various σ levels.

C. Sparse Self FEXT Cancellation Results

The parameters of the simulated vectored VDSL system are listed as follows. The numbers of active downstream (DS) and upstream (US) tones are 1568 and 1209 tones, respectively, the transmitted signal and noise power spectral densities are flat at -60 and -140 dBm/Hz, respectively, the lengths and types of all twisted pairs are 1000 meters and 24-Gauge, respectively, $L = 25$ loops, $B = 4.3125$ KHz, $\Gamma = 13$ dB, $\gamma_c = 3$ dB, $\gamma_m = 6$ dB, and $P_e = 10^{-7}$. We use the analytical model $\left|H^k_{(m,m)}\right|^2 = \exp\left(-1.158\frac{l_m\sqrt{f_k}}{l_o}\right)$ with linear phase for the direct transfer functions [27] where exp(.) is the exponential function, f_k is the frequency of the k^{th} tone in KHz, l_m is the m^{th} loop length in meters, and $l_o = 548.8$ meters is the reference length. For self FEXT, we use the model in [28] where $H^k_{(m,n)} = \left|H^k_{(n,n)}\right| \exp\left(j\phi(f_k)\right) 10^{-0.05\,\rho(f_k)}$ where $j \triangleq \sqrt{-1}$ and $\phi(f_k)$ is a random variable uniformly distributed in the interval $[0, 2\pi]$ radians which models the channel phase dispersion over the k^{th} tone. Furthermore, $\rho(f_k)$ is a Gaussian random variable expressed in dB with standard deviation σ and mean $\mu = 2.33\sigma$ which models the spatial magnitude dispersion of the FEXT coupling channel over the k^{th} tone. The value of σ in dB specifies the spatial coupling dispersion, i.e. as σ increases, the number of dominant crosstalkers decreases and $\bar{\mathbf{H}}$ becomes more sparse. Moreover, if $\sigma = \infty$, $\bar{\mathbf{H}}$ becomes diagonal, i.e. there is no self FEXT. Furthermore, no alien crosstalk is assumed since vectoring is performed over all L pairs in the binder. It can be shown that when $\sigma = 10$ dB, about 90% of the FEXT power originates from just 4 or 5 lines which is typical in practice. Fig. 8 shows the achievable DS and US[4] data rates per line in Mbps versus the active taps percentage in $\widehat{\mathbf{W}}_m$ for various values of σ. For practical values of σ such as $\sigma = 10$ dB, we achieve 50% reduction in run-time complexity at a DS data rate loss of only 0.59 Mbps per line. The achievable data rates of all lines will be the same because they are all assumed to have the same length.

[4]We use the frequency plan and the tone assignment in [29].

VII. Conclusion

We proposed a novel approach for sparse FIR filter design and applied it to three broadband communication scenarios. First, we formulated convex programs and greedy algorithms to design sparse fractionally-spaced FIR LEs, SISO-DFEs, and MIMO-DFEs where dramatic complexity reductions are achieved at a small performance loss compared to the conventional MMSE non-sparse FIR equalizer design. Second, we proposed a novel approach to design the TIR for the channel shortening problem by allowing the TIR taps to be noncontiguous to have a larger search space for the TIR taps. The new sparse TIR design was shown to yield a lower channel shortening MSE compared to the conventional MMSE contiguous TIR design. Third, we designed a per-tone partial self-FEXT canceler for vectored VDSL systems where only a subset of the cancellation taps is activated resulting in substantial complexity reductions. We demonstrate a significant reduction in crosstalk cancellation complexity at small data rate losses compared to theoretical limits.

Acknowledgement

The second author acknowledges financial support by Xtendwave Inc. for the research on the DSL backhaul application reported in Section V. We also thank Mohamed Mokhtar for the discussion about the sparse beamforimg problem.

References

[1] M. Melvasalo, P. Janis, and V. Koivunen, "Sparse equalization in high data rate WCDMA systems," in *IEEE SPAWC*, June 2007.
[2] S. Ariyavisitakul, N. Sollenberger, and L. Greenstein, "Tap-selectable decision feedback equalization," *IEEE Trans. Commun.*, vol. 45, pp. 1497-1500, 1997.
[3] N. Al-Dhahir and C. Fragouli, "How to choose the number of taps in a DFE," in *Proc. CISS*, Mar. 2002.
[4] N. Al-Dhahir and A. Sayed, "The finite-length multi-input multi-output MMSE-DFE," *IEEE Trans. Signal Process.*, vol. 48, pp. 2921-2936, 2000.
[5] A. Gomaa and N. Al-Dhahir, "Sparse FIR equalization: A new design framework," *Submitted for conference publication*.
[6] G. Kutz and D. Raphaeli, "Determination of tap positions for sparse equalizers," *IEEE Trans. Commun.*, vol. 55, no. 9, pp. 1712-1724, 2007.
[7] H. Sui, E. Masry, and B. Rao, "Chip-level DS-CDMA downlink interference suppression with optimized finger placement," *IEEE Trans. Signal Process.*, vol. 54, no. 10, pp. 3908-3921, 2006.
[8] T. Baran, D. Wei, and A. Oppenheim, "Linear programming algorithms for sparse filter design," *IEEE Trans. Signal Process.*, vol. 58, no. 3, pp. 1605-1617, 2010.
[9] N. Al-Dhahir and J. M. Cioffi, "Efficiently computed reduced-parameter input-aided MMSE equalizers for ML detection: A unified approach," *IEEE Trans. Inf. Theory*, vol. 42, pp. 903-915, 1996.
[10] N. Al-Dhahir, "FIR Channel-Shortening Equalizers for MIMO ISI Channels," *IEEE Trans. Commun.*, vol. 49, pp. 213-218, 2001.
[11] S. Roy, T. Duman, and V. McDonald, "Error rate improvement in underwater MIMO communications using sparse partial response equalization," *IEEE J. Ocean. Eng.*, vol. 34, no. 2, pp. 181-201, 2009.
[12] J. Cioffi, V. Oksman, J. Werner, T. Pollet, P. Spruyt, J. Chow, and K. Jacobsen, "Very-high-speed digital subscriber lines," *IEEE Commun. Mag.*, vol. 37, pp. 72-79, 1999.
[13] G. Ginis and J. Cioffi, "Vectored transmission for digital subscriber line systems," *IEEE J. Sel. Areas Commun.*, vol. 20, pp. 1085-1104, 2002.
[14] R. Cendrillon, M. Moonen, G. Ginis, K. V. Acker, T. Bostoen, and P. Vandaele, "Partial crosstalk cancellation for upstream VDSL," *EURASIP J. Appl. Signal Process.*, vol. 10, pp. 1520-1535, 2004.
[15] S. Mallat, G. Davis, and Z. Zhang, "Adaptive time-frequency decompositions," *SPIE J. Optical Eng.*, vol. 33, pp. 2183-2191, 1994.
[16] S. Chen, S. Billings, and W. Luo, "Orthogonal least squares methods and their application to non-linear system identification," *International J. Control*, vol. 50, no. 5, pp. 1873-1896, 1989.
[17] D. Needell and J. Tropp, "CoSaMP: Iterative signal recovery from incomplete and inaccurate samples," *Appl. Computational Harmonic Analysis*.
[18] D. Donoho, "Compressed Sensing," *IEEE Trans. Inf. Theory*, vol. 52, no. 4, pp. 1289-1306, Apr. 2006.
[19] R. Horn and C. Johnson, *Matrix Analysis*. NY, USA: Cambridge Univ. Press, 2009.
[20] N. Al-Dhahir and J. Cioffi, "MMSE decision-feedback equalizer: finite-length results," *IEEE Trans. Inf. Theory*, vol. 41, pp. 961-975, 1995.
[21] J. Cioffi, *EE379A notes, Chapter 3*. Stanford University, USA.
[22] A. Gomaa and N. Al-Dhahir, "Low-complexity sparse FIR channel shortening," in *IEEE GLOBECOM*, 2010.
[23] I. Kalet and S. Shamai, "The next challenge for cellular networks: Backhaul," *IEEE Microwave Mag.*, vol. 10, pp. 54-66, 2009.
[24] J. Cioffi, "A multicarrier primer," ANSI T1E1.4 Committee. Contribution, no. 91-157, Boca Raton, FL, Nov. 1991.
[25] "Guidelines for The evaluation of radio transmission technologies for IMT-2000," *Recommendation ITU-R M.1225*, 1997.
[26] N. Benvenuto and R. Marchesani, "The Viterbi algorithm for sparse channels," *IEEE Trans. Commun.*, vol. 44, pp. 287-289, 1996.
[27] I. Kalet and S. Shamai, "On the capacity of a twisted-wire pair: Gaussian model," *IEEE Trans. Commun.*, vol. 38, pp. 379-383, 1990.
[28] M. Sorbara, P. Duvaut, F. Shmulyian, S. Singh, and A. Mahadevan, "Construction of a DSL-MIMO channel model for evaluation of FEXT cancellation systems in VDSL2," in *IEEE Sarnoff Symp.*, 2007.
[29] "Very high speed digital subscriber line transceivers 2 (VDSL2)," *ITU-T Recommendation G.993.2*, Feb. 2006.

Ahmad Gomaa (S'09) received his B.S and M.S degrees in electronics and communications engineering from Cairo University, Egypt, in 2005 and 2008, respectively. He is currently pursuing the Ph.D. degree at the University of Texas at Dallas, USA. His research interests include sparse FIR filters design, RF impairments compensation at the baseband, training sequence design for channel estimation, and compressive sensing applications to digital communications.

Naofal Al-Dhahir (F'08) is a Jonsson Distinguished Professor of Engineering at the University of Texas at Dallas and an IEEE Fellow. More information is available at http://www.utdallas.edu/∼aldhahir.